International Journal of Mass Spectrometry 313 (2012) 8–14

Contents lists available at SciVerse ScienceDirect

International Journal of Mass Spectrometry

journal homepage: www.elsevier.com/locate/ijms

Static-mirror ion capture and time focusing for electrostatic ion-beam traps and multi-reflection time-of-flight mass analyzers by use of an in-trap potential lift

Robert N. Wolf*, Gerrit Marx, Marco Rosenbusch, Lutz Schweikhard

Institute of Physics, Ernst-Moritz-Arndt University of Greifswald, Felix-Hausdorff-Str. 6, D-17489 Greifswald, Germany

ARTICLE INFO

Article history:
Received 23 November 2011
Received in revised form
12 December 2011
Accepted 13 December 2011
Available online 22 December 2011

Keywords:
Multi-reflection time-of-flight mass spectrometer
Ion-bunch separation
Isobar separation
Electrostatic ion-beam trap
Pulsed drift tube

ABSTRACT

Capture and ejection of ions in electrostatic ion-beam traps and multi-reflection time-of-flight (MR-ToF) devices can be accomplished by pulsing the potential of only a single drift tube inside of the device in contrast to the conventional switching of the ion-mirror voltages. In addition to its simplicity, the new method allows to set the position of the time-focus plane at a given ion detector or ion-beam separator without the need of any further hardware. The position can be adjusted easily by the choice of the pulse height of the potential switch.

1. Introduction

Electrostatic ion-beam traps are a recent development in the area of ion storage devices [1,2]. Similar to electrostatic ion storage rings [3–10] they provide confinement for ions of defined kinetic energies, independent of their mass. Although they are used for various applications in atomic and molecular science [11–17], electrostatic ion-beam traps are based on similar designs and operation principles. Typically, they consist of two ion-optical mirrors creating a potential barrier $qU(z)$ (with the ion charge q and the electric potential $U(z)$ as a function of position along the axis, z) at the ends of a drift section. To achieve storage the potential maxima have to exceed the ions' total energy, i.e., their kinetic energy E in the drift section,

$$qU(z) > E \tag{1}$$

with the potential energy in the drift section defined as zero. Thus, the ions are confined axially and bounce back and forth between the two ion mirrors, see Fig. 1. Transversal confinement is achieved by focusing elements in front of or integrated in the mirrors.

Such an arrangement was already reported five decades ago as "Farvitron" [18,19]. The two electrostatic mirrors were adjusted for identical revolution time independent of the ions initial parameters (for ions of the same mass-to-charge ratio). The ions were produced between the mirrors, i.e., already inside of the device and thus no voltage switching was necessary for the capture. This device was developed as a compact residual-gas analyzer in the UHV range. A related design was later proposed by Wollnik and Przewloka [20] to enhance the performance of ToF mass spectrometers. In this application the ions fly along the same track multiple times while repeatedly being focused by two reflectron ion mirrors in an antiparallel, coaxial configuration. These multi-reflection ToF mass analyzers/spectrometers (MR-ToF MS) were later set up and successfully tested [21–24]. For appropriate electrode arrangements and voltages, high mass-spectral resolving powers $R = m/\Delta m$ have been reached [25–30] which make these devices attractive for precision mass spectrometry and the purification of ion ensembles with respect to their masses [28–30]. In the following we will not distinguish between the various applications and refer to all devices as MR-ToF MS.

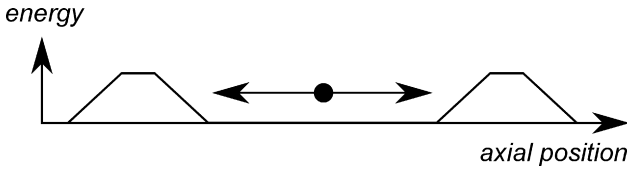

Fig. 1. Schematic illustration of the trapping criterion Eq. (1). Ions are confined axially between the two ion mirrors as long as their kinetic energy is lower than the potential maximum in the mirrors.

* Corresponding author.
E-mail address: wolf@uni-greifswald.de (R.N. Wolf).

1387-3806/$ – see front matter © 2011 Elsevier B.V. All rights reserved.
doi:10.1016/j.ijms.2011.12.006

While in the case of the Farvitron the ions were created inside the trap they are nowadays in general produced in dedicated sources outside of the MR-ToF MS. Thus, they have to be injected into the device by sending them through one of the ion mirrors (the entrance mirror). Similarly, in most cases, the ions are finally ejected through a mirror (exit mirror) for detection or additional investigation. Entrance and exit mirrors may be identical, but in any case, during both injection and ejection, the total ion energy has to be higher than the maximum potential energy in the entrance/exit mirror in order to allow the ion passage. However, this is in contradiction to the trapping criterion, Eq. (1), i.e., different voltage settings are required for the storage and injection/extraction periods of an experimental sequence.

Injection and ejection of ions from MR-ToF MS has been achieved by switching the electric potentials of the entrance and exit mirrors, respectively, to appropriate lower values while the ions are passing. In the following, an alternative method is presented that simplifies the ion transfer to and from the MR-ToF MS considerably: instead of lowering a sufficient number of mirror electrodes, a single capture pulse is applied to just one drift tube between the ion mirrors. In addition, by varying the height of this voltage pulse applied to the in-trap drift tube, the ions' time focus can be adjusted with respect to the distance from the trapping region. Thus, by use of appropriate settings the resolving power for mass spectrometry or for the separation of particular ions of interest from contaminant species can be maximized. Furthermore, by use of the new in-trap potential-lift technique the trapping energy inside the MR-ToF device becomes independent of the transfer energy in the up-/downstream beamline. This decoupling of the MR-ToF MS from the beamline has several advantages, in particular with respect to their individual optimizations. Moreover, it is not necessary that injection and ejection pulses are of equal height which gives the possibility to change the kinetic energy after the MR-ToF device. In the following these features will be discussed in detail.

2. Comparison of ion capturing and ejection with switched mirrors and in-trap lift

Fig. 2 illustrates the differences between the conventional mirror-switching technique (Fig. 2 left) and the in-trap potential-lift technique (Fig. 2 right).

2.1. Mirror switching

When the ion bunch arrives from the left, the potential of the entrance mirror is lowered such that the ions can pass the mirror and enter the trap region (a). After the ions passed the entrance mirror region, the mirror is raised back to the trapping value (b). Thus, externally created ions are captured (c). Similarly, the potential of the exit mirror is lowered below the total ion energy for ejection (d) and ions can escape via the exit mirror (e).

2.2. In-trap lift switching

In the framework of the new in-trap potential-lift method, the incoming ions have a kinetic energy $qU_{\mathrm{transfer}} > qU(z)$ that exceeds the maxima of the mirror potentials. Thus, they pass the first mirror and enter the drift tube from the left (a). While the in-trap lift is activated, i.e., a potential U_{lift} is applied, their kinetic energy is reduced by qU_{lift} when entering the lift electrode. Once the ions have entered the lift it is deactivated, i.e., it is switched to ground potential, (b) and the ions are trapped as their energy is no longer high enough to pass the mirrors (c). After a certain number of reflections, the ions can be ejected by activating the in-trap lift voltage again while they are inside the drift tube (d). Thus, they are regaining enough energy to leave the MR-ToF MS (e).

Due to the strong focusing effect of the inhomogeneous electric field inside the mirror, special care has to be taken with respect to the injection ion optics in front of the device and the ejection ion optics behind the device. As an example a set of cylindrical lenses can be used to focus the beam near the turn-around point to prevent radial ion losses.

2.3. Comparison

The use of the in-trap potential lift instead of switched mirrors has several advantages. The nominal trapping energy inside the MR-ToF device becomes decoupled from the transfer energy of the beamlines in front and behind the MR-ToF MS. As long as the transfer energy of the ions in the beamline is high enough to let the ions pass the mirrors, they can be captured with the in-trap lift to any nominal trapping energy below the transfer energy. This simplifies the optimization of antecedent parts of the MR-ToF MS, because changing the transfer energy qU_{transfer} does not affect the trapping conditions as long as the difference $U_{\mathrm{transfer}} - U_{\mathrm{lift}}$ is kept

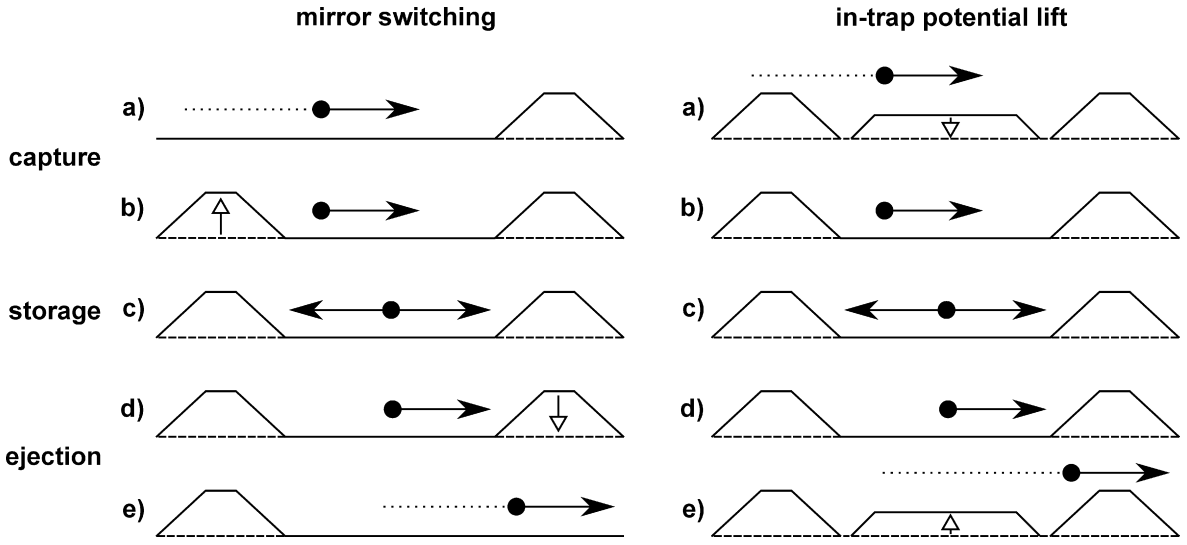

Fig. 2. Schematic illustration of ion capture, storage and ejection with a mirror-switching design (left) and with a static mirror design using an in-trap potential lift (right). For details see text.

constant. On the other hand, the nominal trapping energy can be varied without the need of adjusting the ion-source potential or other ion-optical elements outside the MR-ToF MS. In addition, the tuning of the trapping energy is a very effective and efficient way to maximize the resolving power, as described in the next section.

On the other hand, the in-trap lift reduces the accepted time-of-flight distance of different species or, in case of extended bunches or continuous ion beams, the trapped number of ions. Depending on the particular layout of the device, the in-trap lift has a length of l_{lift} and incoming ions have a kinetic energy of E. The time of flight they travel through the lift electrode is

$$t_{\mathrm{lift}} = \frac{l_{\mathrm{lift}}}{v} = l_{\mathrm{lift}} \cdot \sqrt{\frac{m}{2E}}. \tag{2}$$

For example, the velocity of light ions with a mass of $m = 28$ u and a kinetic energy of $E = 2$ keV is $v \approx 120\ \mathrm{mm\ \mu s^{-1}}$. Thus they need $t_{\mathrm{lift}} \approx 2.6\ \mu$s to pass a $l_{\mathrm{lift}} = 300$ mm drift tube. Edge effects have not been included in the present study. The edge field region of about one to two times the drift-tube diameter should be avoided, i.e., no ions should be within this region when the voltage is switched since they would acquire a different energy, between $q(U_{\mathrm{transfer}} - U_{\mathrm{lift}})$ and qU_{transfer}. Using fast solid-state switches with transition times well below 0.1 μs, the accepted time-of-flight distance is close to the drift time in the lift electrode minus the edge regions. Furthermore, ions that are far enough away from the accelerating or decelerating edge regions used to increase or decrease the ions' kinetic energy for ejection or injection (either in the mirror regions or somewhere else in the drift tube) are not affected by potential changes of the in-trap lift electrode. Therefore, once the distance between two species is large enough, only one of them can be addressed selectively for ejection or capturing.

The main difficulty in using an MR-ToF device for high mass-resolving power is to keep the mirror voltages as constant as possible over the whole measurement period. In general, the power supplies produce voltage fluctuations ranging from several hundreds of kilohertz down to a few microhertz. High-frequency fluctuation, ripple or noise is produced by the transformers used to create high voltages. On top of that, there may be a 50/60 Hz component originating from line voltage. This contribution is usually well known and specified for the device. In contrast, the low-frequency fluctuations or drifts below 1 Hz are often unknown. They are, in general, much higher in amplitude than the high-frequency components and very hard to suppress.

One has to distinguish, which of these components degrade the performance of the device in which state of operation. The high-frequency components change the potential distribution inside the mirrors in the time range of the ions' revolution time. Thus, they decrease the mass-resolving power achieved for a single-shot spectrum. The mid-frequency fluctuations change the potential distribution between several spectra, assuming experimental repetition rates between about 1 Hz and 1 kHz. This leads to a blurred accumulated spectrum that is often several times worse than the single-shot spectra. The low-frequency contributions change focusing and arrival times in the range of minutes to hours, which needs to be compensated by continuous recalibration and reoptimization of the apparatus.

There is an additional difficulty connected with the switching of the mirrors: Their potential distribution changes as a function of time after the mirror voltages are switched on. This is due to the drop of the high-voltage line caused by the load change, which is then compensated by the power-supply biasing the mirror-electrode voltage. Thus, there is a different optimal trapping potential distribution that compensates ToF aberrations best for every number of revolutions n. For an optimization of the resolving power the mirror-potential distribution has to be re-adjusted for each specific number of revolutions.

As an example, assume a mirror electrode switched from 0 for injection to V_{nom} nominal trapping voltage and a capacitance of the load circuitry of C_{load}. To recharge the electrode within a few hundred nanoseconds, an energy storage in form of a buffer capacitor may be used, for example $C_{\mathrm{buffer}} = 100 \cdot C_{\mathrm{load}}$. After switching, the electrode is only recharged to $V = V_{\mathrm{nom}} \cdot C_{\mathrm{buffer}}/(C_{\mathrm{buffer}} + C_{\mathrm{load}}) = 0.99 \cdot V_{\mathrm{nom}}$. This voltage drop of 1% is then recharged by the powersupply, leading to a voltage change typically in the millisecond range, dependent on the current output and regulation speed of the power supply. Therefore, the potential distribution inside the mirror changes continuously for milliseconds, which decreases the performance considerably. In contrast, the in-trap lift is free from this drawback. The ions are only influenced by the pulsed drift electrode when they are entering or leaving the MR-ToF MS. This period is very short, of the order of a microsecond, and thus power-supply drifts due to load changes are negligible.

3. Time-of-flight focusing

To maximize the resolving power of a ToF MS, it is most important to control the position of the time-focus plane. Ideally, for mass analysis or ion separation it is placed on the detector or on the device for ion selection, respectively. The time-focus plane of an arbitrary ion source can be shifted in space by use of a reflectron [31] as well as by a multi-reflection ToF device as discussed in the following.

Ions (of the same mass-over-charge ratio) oscillate in an MR-ToF MS with a revolution time $T(E)$ depending on their kinetic energy E. More quantitatively, the relative revolution-time difference

$$\delta_T = \frac{T}{T_0} - 1 \tag{3}$$

of any ion with respect to a reference ion with a period T_0 can be expressed as a function of its relative kinetic-energy difference

$$\delta_E = \frac{E}{E_0} - 1 \tag{4}$$

with respect to the reference ion's kinetic energy E_0. In the following, small deviations ($\delta_T \ll 1$, $\delta_E \ll 1$) are assumed which allows to limit the discussion about the energy dependent ToF differences to the linear coefficient $\partial\delta_T/\partial\delta_E$. Moreover, ToF aberrations with respect to geometric deviations are not considered, i.e., the ions are assumed to fly close to the optical axis of the system (for a more detailed treatment, see references [24,25,31]). The settings can either be adjusted to $\partial\delta_T/\partial\delta_E > 0$, i.e., ions with higher energy have a longer revolution time or to $\partial\delta_T/\partial\delta_E < 0$, i.e., ions with lower energy having a longer revolution time. Both of these cases can be achieved in an MR-ToF device either by adjusting the mirror-potentials for a fixed kinetic energy or by adjusting the kinetic energy for fixed mirror potentials. The latter is illustrated in Fig. 3. It is considerably easier than the first method as there is no need to adjust the mirror voltages once these values have been optimized. Depending on the value of $\partial\delta_T/\partial\delta_E$, the position of the time-focus plane of the MR-ToF device will change: For $\partial\delta_T/\partial\delta_E < 0$, it moves closer to and for $\partial\delta_T/\partial\delta_E > 0$ further away from the ion source. With the in-trap lift, the average trapping energy of an ion bunch is chosen when the ions enter the devices, $E = q(U_{\mathrm{transfer}} - U_{\mathrm{lift}} \pm \Delta U)$. In other words, the in-trap lift aides to navigate the ion bunch on the $\delta_T(\delta_E)$ curve, see Fig. 3.

Most MR-ToF mirror-potential optimizations aim at the energy-isochronous state $\partial\delta_T/\partial\delta_E = 0$ [22–30]. However, this condition is usually not easily achieved and conserved. In contrast, it will be shown in the following that states with $\partial\delta_T/\partial\delta_E \neq 0$ can be used to gain a comparably high mass-resolving power. In addition, this method relies on the variation of only one voltage which favors

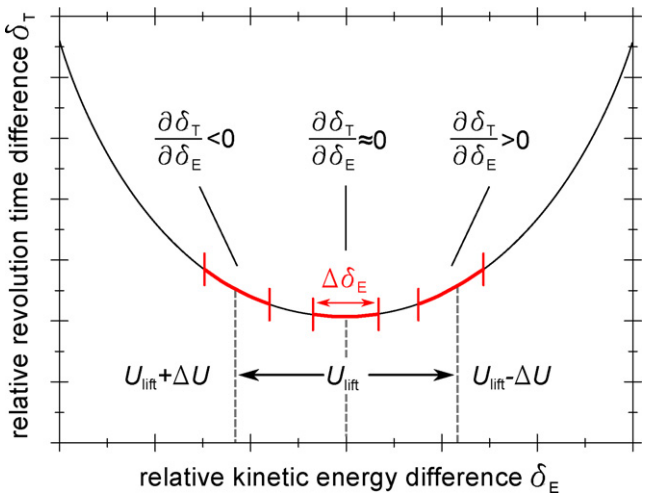

Fig. 3. Schematic example of the relative revolution-time difference δ_T as a function of the relative kinetic-energy difference δ_E. Sections of different slopes are indicated in red as well as the energy distribution $\Delta\delta_E$ of a bunch. To change the average kinetic energy of a bunch and therefore the corresponding ToF energy dispersion relation $\partial\delta_T/\partial\delta_E$, the in-trap potential lift voltage U_{lift} can be changed.

a quick optimization of an MR-ToF device. Moreover, for each number of revolutions n and each position of the ion source's time-focus plane, an optimal time focusing of the MR-ToF device can be achieved as long as there is a change in sign of $\partial\delta_T/\partial\delta_E$. The two cases of a positive and a negative ToF energy-dispersion coefficient are discussed in the following.

3.1. Positive ToF energy-dispersion coefficient, $\partial\delta_T/\partial\delta_E > 0$

Fig. 4 illustrates the case where the time-focus position of the ion source is located in front of the MR-ToF device. At passing this plane, the faster ions outpace the slower ions and the signal width Δt of the ion bunch starts to increase again due to the different kinetic energies originating from different axial starting positions in the ion source. Within the flight time t_1 from the time-focus position of the source to the center of the MR-ToF device, the time spread increases by Δt_1 and in the flight time t_2 from the center of the MR-ToF device to the detector by Δt_2. By capturing the ion bunch and storing at a kinetic trapping energy with positive energy-dispersion coefficient $\partial\delta_T/\partial\delta_E > 0$ (Fig. 3), the time difference between ions of different kinetic energies becomes smaller with each revolution. After a certain number of revolutions, i, a second time-focus plane can be found in the center of the device (Fig. 4 middle), i.e., the ToF deviation Δt_1 is compensated. However, after the ions are released towards the detector, they will again start to spread in time (Fig. 4 middle, right). Therefore, to compensate the ToF difference Δt_2 due to the flight path from the center of the analyzer to the detector, an additional number of revolutions j has to be performed before the ions are ejected (Fig. 4, bottom).

Let $\Delta t_s = \Delta t_1 + \Delta t_2$ be the ToF difference between the slowest and the fastest ion at the detector plane while "shooting through" the MR-ToF device with an activated in-trap lift (Fig. 4 top). This time difference has to be compensated in $n = i + j$ revolutions, thus $\Delta t_s/n$ per revolution. This leads to

$$\frac{\Delta t_s}{n} \stackrel{!}{=} T_0 \frac{\partial\delta_T}{\partial\delta_E}\Delta\delta_E \tag{5}$$

to compensate the ToF deviation with respect to energy.

To achieve a high mass-resolving power

$$R = \frac{m}{\Delta m} = \frac{t}{2\Delta t}, \tag{6}$$

the absolute flight time $t = t_1 + nT_0 + t_2 = t_s + nT_0$ has to be high compared to the ToF distribution Δt at the detector plane. When the ToF deviations Δt_s originating from energy differences $\Delta\delta_E$ and initial ToF differences Δt_{th} (thermal ion distribution in source region, turn-around time in pulsed ion converters) are add up, the overall ToF distribution width is

$$\Delta t = \sqrt{\Delta t_{th}^2 + \left(\Delta t_s - nT_0 \frac{\partial\delta_T}{\partial\delta_E}\Delta\delta_E\right)^2} \tag{7}$$

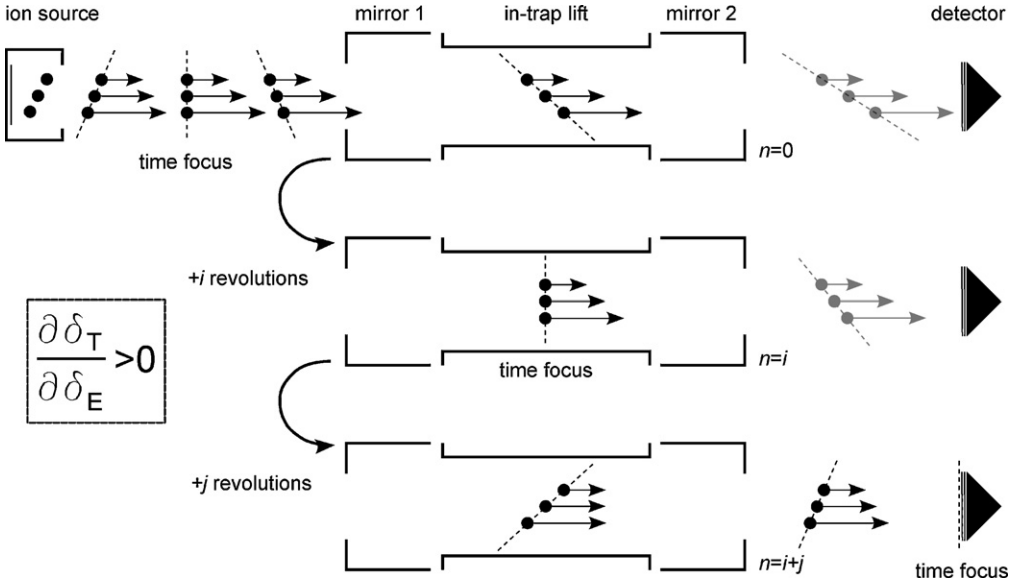

Fig. 4. Illustration of the time focusing by use of the in-trap lift for a positive ToF energy dispersion coefficient. The ion source's time-focus plane is located between the ion source and the MR-ToF device. After i revolutions, a time focus plane is found in the middle plane of the MR-ToF and after $i + j$ revolutions, the time focus has moved onto the detector. For further explanations see text.

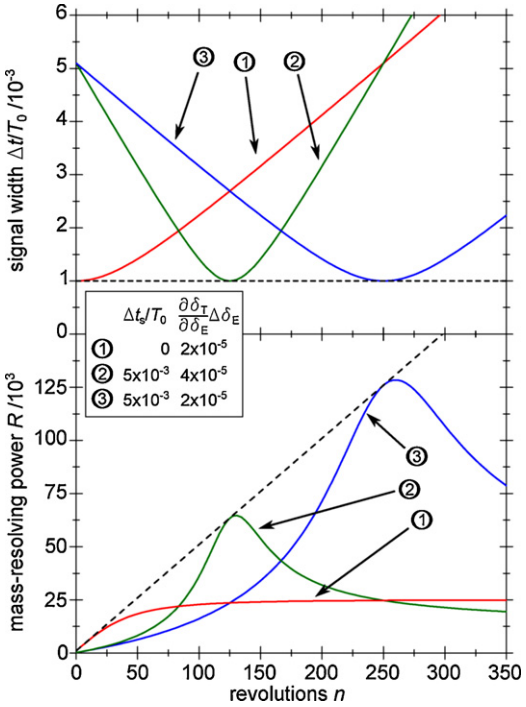

Fig. 5. Relative time width (top) and mass-resolving power (bottom) as a function of the number of revolutions according to Eqs. (8) and (9), respectively (for $t_s/T_0 = 2$ and $\Delta t_{th}/T_0 = 1 \times 10^{-3}$). The curves represent three sets of ToF energy dispersions $\partial\delta_T/\partial\delta_E \cdot \Delta\delta_E$ and time spreads $\Delta t_s/T_0$, the dashed curve represents the case of a ToF energy-isochronous state.

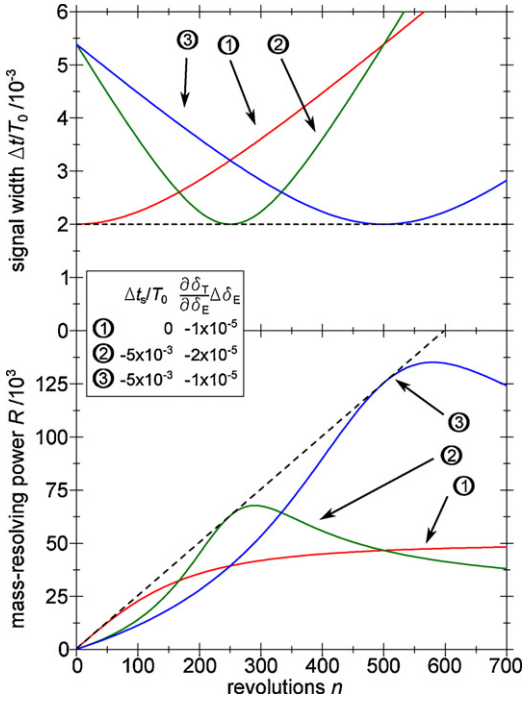

Fig. 6. Relative time width (top) and mass-resolving power (bottom) as a function of the number of revolutions according to Eqs. (8) and (9), respectively (for $t_s/T_0 = 2$, $\Delta t_{th}/T_0 = 2 \times 10^{-3}$). The curves represent three sets of different ToF energy dispersions $\partial\delta_T/\partial\delta_E \cdot \Delta\delta_E$ and time spreads $\Delta t_s/T_0$, the dashed curve represents the case of a ToF energy-isochronous state. Note the changed abscissa compared to Fig. 5.

which results in a mass-resolving power

$$R = \frac{m}{\Delta m} = \frac{t}{2\Delta t} = \frac{t_s + nT_0}{2\sqrt{\Delta t_{th}^2 + (\Delta t_s - nT_0(\partial\delta_T/\partial\delta_E)\Delta\delta_E)^2}}. \quad (8)$$

Fig. 5 shows the relative ToF distribution width

$$\frac{\Delta t}{T_0} = \sqrt{\frac{\Delta t_{th}^2}{T_0^2} + \left(\frac{\Delta t_s}{T_0} - n\frac{\partial\delta_T}{\partial\delta_E}\Delta\delta_E\right)^2} \quad (9)$$

and the mass-resolving power R as a function of the number of revolutions inside the MR-ToF device.

The first curve (red) exemplifies the cases when the time-focus plane of the ion source was initially set on the detector, $\Delta t_s = 0$, and the ions with an energy difference $\Delta\delta_E$ are confined in the MR-ToF with a weak positive ToF energy dispersion, $\partial\delta_T/\partial\delta_E \cdot \Delta\delta_E = 2 \times 10^{-5}$. In this case, the signal width is increasing continuously, starting from its minimal value, i.e., the thermal time spread $\Delta t_{th} = 10^{-3}T_0$ (Fig. 5 top). This induces a fast, quasi-linear increase in mass-resolving power for the first few tens of revolutions until it converges slowly to the maximum for higher revolution numbers (Fig. 5 bottom). This maximum, for $n \to \infty$, is limited by the ToF energy dispersion $\partial\delta_T/\partial\delta_E \cdot \Delta\delta_E$. For the second (green) and third (blue) curves, different ToF energy coefficients and relative energy differences $\partial\delta_T/\partial\delta_E \cdot \Delta\delta_E$ were chosen for a fixed initial time-focus plane in front of the detector, such as the primary time focus position of the ion source. The ToF from this plane to the detector was set to $t_s = 2T_0$ and the ToF difference was chosen as $\Delta t_s = 5 \times 10^{-3}T_0$. The initially high time spread Δt is reduced until a minimum, namely Δt_{th}, is obtained according to

$$\frac{\partial\Delta t(n)}{\partial n} \stackrel{!}{=} 0 \quad (10)$$

after

$$n_{\Delta t} = \frac{\Delta t_s}{T_0}\frac{1}{(\partial\delta_T/\partial\delta_E)\Delta\delta_E} \quad (11)$$

revolutions where a mass-resolving power of

$$R(n_{\Delta t}) = \frac{t_s + n_{\Delta t}T_0}{2\Delta t_{th}} = \frac{1}{2\Delta t_{th}}\left(t_s + \frac{\Delta t_s}{(\partial\delta_T/\partial\delta_E)\Delta\delta_E}\right) \quad (12)$$

is reached. The maximum of the mass-resolving power is derived from

$$\frac{\partial R(n)}{\partial n} \stackrel{!}{=} 0 \quad (13)$$

and is reached at

$$n_R = n_{\Delta t}\left(1 + \frac{\Delta t_{th}^2}{\Delta t_s(\Delta t_s + t_s(\partial\delta_T/\partial\delta_E)\Delta\delta_E)}\right) \quad (14)$$

revolutions with a value of

$$\begin{aligned} R(n_R) &= \frac{1}{2(\partial\delta_T/\partial\delta_E)\Delta\delta_E}\sqrt{\left(\frac{\Delta t_s + t_s(\partial\delta_T/\partial\delta_E)\Delta\delta_E}{\Delta t_{th}}\right)^2 + 1} \\ &= R(n_{\Delta t})\sqrt{\left(\frac{\Delta t_{th}}{\Delta t_s + t_s(\partial\delta_T/\partial\delta_E)\Delta\delta_E}\right)^2 + 1} \\ &= R(n_{\Delta t}) + \frac{1}{2}R(n_{\Delta t})\left(\frac{\Delta t_{th}}{\Delta t_s + t_s(\partial\delta_T/\partial\delta_E)\Delta\delta_E}\right)^2 - \dots \end{aligned} \quad (15)$$

In comparison to case 1 of Fig. 5, i.e., an ion-source time-focus position initially set on the detector and an MR-ToF with a weak positive ToF energy-dispersion coefficient where a maximum mass-resolving power of $R \approx 25,000$ is approached asymptotically, in case 2 the maximum $R \approx 65,000$ is reached at only $n_R \approx 130$ revolutions. This holds even for a ToF energy-dispersion coefficient further away from the energy-isochronous condition $\partial\delta_T/\partial\delta_E = 0$,

because the minimum time spread $\Delta t = \Delta t_{th}$ is found at a higher number of revolutions, $n_{\Delta t}$, and therefore at a longer flight time $t = t_s + n_{\Delta t} T_0$. In case 3, a mass-resolving power of $R \approx 128,000$ is reached at $n_R \approx 260$ revolutions with the same ToF energy dispersion as in case 1 (particularly the same potential distribution of the MR-ToF mirrors), but with the initial focus point in front of the detector. The number of revolutions were the minimum of Δt is found is proportional to the time spread gained between the ion source's time-focus point and detector, Δt_s, and inverse proportional to the ToF energy dispersion $\partial\delta_T/\partial\delta_E \cdot \Delta\delta_E$, Eq. (11).

3.2. Negative ToF energy-dispersion coefficient, $\partial\delta_T/\partial\delta_E < 0$

In the case that the time-focus plane of the ion source is behind the detector, the MR-ToF device can be operated in a negative-dispersion mode to move this plane onto the detector and achieve maximum mass-resolving power.

All considerations can be performed in analogy to the case discussed above, Section 3.1. Again, Δt_s is the time difference between the slowest and the fastest ion at the detector plane and is now of negative sign because the slowest ion still leads the bunch and therefore has the shortest flight time, $\Delta t_s < 0$. This has to be compensated within n revolutions, analog to Eq. (5). The slowest ions leading the ensemble will now have a higher revolution time inside the MR-ToF and therefore with each revolution the time-focus plane will move closer to the detector. With the given definition of Δt_s, which in this case turns negative, the mass-resolving power and relative ToF distribution width are still expressed by Eqs. (8) and (9). For consistency, the value of t_s is kept the same. The corresponding curves for graphical illustration are shown in Fig. 6. In order to create a focus point behind the detector, the time spread $\Delta t_{th}/T_0 = 2 \times 10^{-3}$ was doubled while the ToF energy dispersions were halved. All other considerations are the same as in the case of positive ToF energy dispersion, discussed above. As a consequence of the reduction of the ToF energy dispersions by a factor of two, the number of revolutions to reach the minimum time spread or maximum mass resolving power is doubled in cases 2 and 3 of Fig. 6.

4. Summary and outlook

By use of a pulsed drift tube between the ion mirrors of an MR-ToF device the operation can be significantly facilitated. Several implications of this approach have been outlined. In particular, there is no lack of mass resolving power with respect to the conventional method of switching of the mirror voltages. Moreover, the mass resolving power can be maximized for any number of revolutions, ion-source configuration and position as well as detector position by adjustment of a single, minor-critical voltage and without the need of further external ion optics. The new method is currently been tested at the on-line mass spectrometer ISOLTRAP [30].

In addition, the single ion description is presently extended by computer simulations including ion–ion interaction. In particular, a possible advantage of the negative dispersion mode may be the avoidance of ion bunch coalescence, previously referred to as self bunching [32–34], where a bunch of ions stays focused in time, regardless of their (close but different) mass-over-charge ratios. This effect of the Coulomb interaction and corresponding energy transfer between the ions is thought to appear in positive dispersion mode only. By avoiding this regime, higher ion numbers could be injected and mass analyzed or separated. Further investigations and comparisons of the modes discussed based on Coulomb-interaction simulations are currently under way.

Acknowledgment

This work was supported by the German Federal Ministry for Education and Research (BMBF) (06GF186I, 06GF9102 and 06GF9101I).

References

[1] D. Zajfman, O. Heber, L. Vejby-Christensen, I. Ben-Itzhak, M. Rappaport, R. Fishman, M. Dahan, Phys. Rev. A 55 (1997) R1577.
[2] W.H. Benner, Anal. Chem. 69 (1997) 4162.
[3] S.P. Moller, Nucl. Instrum. Methods Phys. Res. A 394 (1997) 281.
[4] T. Tanabe, K. Chida, K. Noda, I. Watanabe, Nucl. Instrum. Methods Phys. Res. A 482 (2002) 595.
[5] C.P. Welsch, J. Ullrich, C. Glässner, A. Schempp, R. Dörner, H. Schmidt-Böcking, Nucl. Instrum. Methods Phys. Res. A 527 (2004) 284.
[6] S. Jinno, T. Takao, Y. Omata, A. Satou, H. Tanuma, T. Azuma, H. Shiromaru, K. Okuno, N. Kobayashi, I. Watanabe, Nucl. Instrum. Methods Phys. Res. A 532 (2004) 477.
[7] D. Zajfman, A. Wolf, D. Schwalm, D.A. Orlov, M. Grieser, R. von Hahn, C.P. Welsch, J.R.C. Lopez-Urrutia, C.D. Schröter, X. Urbain, J. Ullrich, J. Phys.: Conf. Ser. 4 (2005) 296.
[8] J. Bernard, G. Montagne, R. Brédy, B. Terpend-Ordacière, A. Bourgey, M. Kerleroux, L. Chen, H.T. Schmidt, H. Cederquist, S. Martin, Rev. Sci. Instrum. 79 (2008) 075109.
[9] C. Welsch, J. Harasimowicz, K. Kühnel, A. Papash, M. Putignano, P. Schmid, J. Ullrich, Hyperfine Interact. 194 (2009) 137.
[10] R.D. Thomas, H.T. Schmidt, G. Andler, M. Bjorkhage, M. Blom, L. Brannholm, E. Backstrom, H. Danared, S. Das, N. Haag, P. Hallden, F. Hellberg, A.I.S. Holm, H.A.B. Johansson, A. Kallberg, G. Kallersjo, M. Larsson, S. Leontein, L. Liljeby, P. Lofgren, B. Malm, S. Mannervik, M. Masuda, D. Misra, A. Orban, A. Paal, P. Reinhed, K.-G. Rensfelt, S. Rosen, K. Schmidt, F. Seitz, A. Simonsson, J. Weimer, H. Zettergren, H. Cederquist, Rev. Sci. Instrum. 82 (2011) 065112.
[11] M.W. Froese, K. Blaum, F. Fellenberger, M. Grieser, M. Lange, F. Laux, S. Menk, D.A. Orlov, R. Repnow, T. Sieber, Y. Toker, R. von Hahn, A. Wolf, Phys. Rev. A 83 (2011) 023202.
[12] J.B. Greenwood, O. Kelly, C.R. Calvert, M.J. Duffy, R.B. King, L. Belshaw, L. Graham, J.D. Alexander, I.D. Williams, W.A. Bryan, I.C.E. Turcu, C.M. Cacho, E. Springate, Rev. Sci. Instrum. 82 (2011) 043103.
[13] P. Reinhed, A. Orban, S. Rosen, R.D. Thomas, I. Kashperka, H.A.B. Johansson, D. Misra, A. Fardi, L. Brannholm, M. Bjorkhage, H. Cederquist, H.T. Schmidt, Nucl. Instrum. Methods Phys. Res. A 621 (2010) 83.
[14] M. Lange, M. Froese, S. Menk, J. Varju, R. Bastert, K. Blaum, J.R.C. López-Urrutia, F. Fellenberger, M. Grieser, R. von Hahn, O. Heber, K.-U. Kühnel, F. Laux, D.A. Orlov, M.L. Rappaport, R. Repnow, C.D. Schröter, D. Schwalm, A. Shornikov, T. Sieber, Y. Toker, J. Ullrich, A. Wolf, D. Zajfman, Rev. Sci. Instrum. 81 (2010) 055105.
[15] J.D. Alexander, C.R. Calvert, R.B. King, O. Kelly, W.A. Bryan, G.R.A.J. Nemeth, W.R. Newell, C.A. Froud, I.C.E. Turcu, E. Springate, P.A. Orr, J. Pedregosa-Gutierrez, C.W. Walter, R.A. Williams, I.D. Williams, J.B. Greenwood, J. Phys. B 42 (2009) 154027.
[16] P. Reinhed, A. Orban, J. Werner, S. Rosen, R.D. Thomas, I. Kashperka, H.A.B. Johansson, D. Misra, L. Brannholm, M. Bjorkhage, H. Cederquist, H.T. Schmidt, Phys. Rev. Lett. 103 (2009) 213002.
[17] D. Zajfman, Y. Rudich, I. Sagi, D. Strasser, D.W. Savin, S. Goldberg, M. Rappaport, O. Heber, Int. J. Mass Spectrom. 229 (2003) 55.
[18] W. Tretner, Z. Angew. Phys. 11 (1959) 395.
[19] W. Tretner, Vacuum 10 (1960) 31.
[20] H. Wollnik, M. Przewloka, Int. J. Mass Spectrom. Ion Processes 96 (1990) 267.
[21] C. Piyadasa, P. Hakansson, T. Ariyaratne, Rapid Commun. Mass Spectrom. 13 (1999) 620.
[22] C. Scheidenberger, F. Attallah, A. Casares, U. Czok, A. Dodonov, S.A. Eliseev, H. Geissel, M. Hausmann, A. Kholomeev, V. Kozlovski, Y.A. Litvinov, M. Maier, G. Münzenberg, N. Nankov, Y.N. Novikov, T. Radon, J. Stadlmann, H. Weick, M. Weidenmuller, H. Wollnik, Z. Zhou, Hyperfine Interact. 132 (2001) 531.
[23] A. Casares, A. Kholomeev, H. Wollnik, Int. J. Mass Spectrom. 206 (2001) 267.
[24] H. Wollnik, A. Casares, Int. J. Mass Spectrom. 227 (2003) 217.
[25] A. Verentchikov, M. Yavor, Y. Hasin, M. Gavrik, Tech. Phys. 50 (2005) 82.
[26] Y. Ishida, M. Wada, H. Wollnik, Nucl. Instrum. Methods Phys. Res. B 241 (2005) 983.
[27] W.R. Plass, T. Dickel, M. Petrick, D. Boutin, Z. Di, T. Fleckenstein, H. Geissel, C. Jesch, C. Scheidenberger, Z. Wang, Eur. Phys. J. Special Topics 150 (2007) 367.
[28] W.R. Plass, T. Dickel, U. Czok, H. Geissel, M. Petrick, K. Reinheimer, C. Scheidenberger, M.I. Yavor, Nucl. Instrum. Methods Phys. Res. B 266 (2008) 4560.
[29] A. Piechaczek, V. Shchepunov, H. Carter, J. Batchelder, E. Zganjar, S. Liddick, H. Wollnik, Y. Hu, B. Griffith, Nucl. Instrum. Methods Phys. Res. B 266 (2008) 4510.
[30] R.N. Wolf, M. Eritt, G. Marx, L. Schweikhard, Hyperfine Interact. 199 (2011) 115.

[31] M. Yavor, P.W. Hawkes, T. Mulvey (Eds.), Advances in Imaging and Electron Physics: Optics of Charged Particle Analyzers, 1st edition, Elsevier, Amsterdam, 2009.
[32] D. Zajfman, D. Strasser, O. Heber, S. Goldberg, A. Diner, M.L. Rappaport, Nucl. Instrum. Methods Phys. Res. A 532 (2004) 196.
[33] M.W. Froese, M. Lange, S. Menk, M. Grieser, O. Heber, F. Laux, R. Repnow, T. Sieber, Y. Toker, R. von Hahn, A. Wolf, K. Blaum, Bunching properties in a cryogenic electrostatic ion beam trap, New J. Phys., private communication.
[34] P.A. Bolotskikh, D.E. Grinfeld, A.A. Makarov, M.A. Monastyrskiy, Nucl. Instrum. Methods Phys. Res. A 645 (2011) 146.